

Article

Study on the Deformation and Failure Characteristics of the Long Composite Insulated Cold Transmission Pipe in Deep Mines

Wenlong Wang¹, Fengtian Yue², Jingsheng Wei^{3,*}, Tao Gao² and Yanjun Qi^{2,*}

- ¹ State Key Laboratory for Geomechanics and Deep Underground Engineering, China University of Mining and Technology, Xuzhou 221116, China; 4277@cumt.edu.cn
- ² School of Mechanics and Civil Engineering, China University of Mining & Technology, Xuzhou 221116, China
- ³ School of Materials Science and Physics, China University of Mining & Technology, Xuzhou 221116, China
- * Correspondence: wjvictor@163.com (J.W.); cumtqyj@cumt.edu.cn (Y.Q.)

Abstract: To address the delamination and water leakage caused by the fracture of insulated chilled water pipeline (ICWP) in the process of long-distance drilling through deep strata, a new insulated cold transmission pipe with a composite structure was designed based on the actual project. The mechanical and deformation characteristics of the mortar materials of the different filling layers were investigated using uniaxial compression and Brazilian split tests. The distribution law of the maximum principal strain field on the surface during the test process was obtained by applying the digital image correlation method. Based on the experimental results, the finite-difference model was established and FLAC3D was used to analyze the stability of the long-distance composite structure ICWP under different stress conditions. The numerical results show that when the ground stress exceeds 12 MPa, the plastic damage occurs in the inner and outer filling layers of the ICWP. When the ground stress reaches 17.5 MPa, there is a small plastic zone in the cold transmission pipe, but the composite structure ICWP does not affect the regular operation of the pipe. Based on that, the mapping relationship for the plastic damage rate of the inner and outer filling mortar of the ICWP to the ground stress and the parameters of the insulation pipe was constructed to provide a theoretical basis for improving the deformation damage resistance characteristics of the composite structure ICWP.

Keywords: deep mine; long distance; cold transmission pipe; mechanical properties; overall stability



Citation: Wang, W.; Yue, F.; Wei, J.; Gao, T.; Qi, Y. Study on the Deformation and Failure Characteristics of the Long Composite Insulated Cold Transmission Pipe in Deep Mines. *Appl. Sci.* **2023**, *13*, 8805. <https://doi.org/10.3390/app13158805>

Academic Editors: Chun Zhu, Yujun Zuo, Shibin Tang and Qian Yin

Received: 19 May 2023
Revised: 27 July 2023
Accepted: 28 July 2023
Published: 30 July 2023



Copyright: © 2023 by the authors. Licensee MDPI, Basel, Switzerland. This article is an open access article distributed under the terms and conditions of the Creative Commons Attribution (CC BY) license (<https://creativecommons.org/licenses/by/4.0/>).

1. Introduction

With the expansion of population and rapid industrialization, more minerals need to meet the rapidly growing demand for resources [1], which requires the excavation of deep underground minerals. In 2015, there were more than 74 coal mines with a mining depth exceeding 900 m, and the original raw rock temperature ranges from 35 to 45 °C in China. Recently, an increasing number of coal and metal mines have engineering challenges caused by hot and humid mining environments, adversely impacting the health of miners, mining facilities, and productive force [2].

To create the thermal environment required for the underground space, a running system that improves overall efficiency and reduces electricity costs was adopted [3–5]. Surface air coolers, 0 °C chilled water, and an ice cooling system were used to explore energy-saving solutions for deep mines [6]. Inrushing mine water was used as the cooling energy to control the environment, which helped to reduce the energy consumption of the cooling system [7].

The cooling system consumes more than 20% of the total energy in the mine. Using variable speed drive technology decreases electricity demand, thus reducing 33% of the total energy consumption [8,9]. The thermal-hydraulic characteristics of the mine cooling system were studied by evaluating the energy consumption of the system with a simulation

model in a holistic view. The results showed that creating a comfortable and healthy environment is possible without a significant increase in capital costs [10].

Although the above survey shows that these technologies can reduce electricity cost, the investment and electricity consumption of the cooling system is quite high for a mine. That is because a large amount of heat transfers from the surrounding rock to the airflow in the deep underground space, resulting in an increased cooling load. By insulating the building envelope, the cooling load can be reduced, thus cutting the electricity cost and investment of the cooling system [11–13]. The use of thermal insulation materials can reduce the overall energy consumption of cooling systems in the underground space [14]. Heat transferred from the surrounding rock to the underground space may account for more than 75% of the total cooling load in deep mines [15]. By analyzing the effect of the thermal insulating layer on the surrounding rock heat radiation, we concluded that the heat flux between the surrounding rock and the airflow can be reduced by using thermal insulation materials. The total cost associated with thermal insulation first decreases and then increases when the insulation thickness increases [16].

Currently, air conditioning technology is mainly used for mine cooling, improving the thermal and humid environment of the mine tunnel and working face by directly controlling the temperature and humidity of the airflow in the mine. There are three kinds of cooling systems: the ground-chilled water system [4], the underground-chilled water system [5], and the ground ice slurry system [6]. The three kinds of cooling systems need to transport different secondary refrigerants to the underground through the piping system to ensure that the refrigerant temperature meets the refrigeration and energy-saving requirements. Mine cooling systems can make up to 25% of a mine's total electricity consumption [17]. The coefficient of performance (COP) of the ice slurry cooling system is usually lower than the water cooling system [4]. He et al. [18] proposed the HEMS technology of high-temperature heat-harm control in deep mining with the constant temperature layer water source as the refrigerant, which achieved a good cooling effect in the mine with good water source conditions.

Under the guidance of carbon peaking and carbon neutrality policy, the cooling technology of cold water in heat-damaged mines is bound to receive better development in China. Feng et al. [19] proposed a maximum air volume cooling system in which the air supply was cooled directly on the surface. The cooling effect is better in the initial stage of the heat-damaged mine and in the mine with the short mining distance.

However, no more mature mine cooling research results can be widely promoted due to the differences in the causes of heat damage in mines in practice, underground mining methods, mechanical and electrical equipment configurations, and ventilation systems. The use of artificial refrigeration cooling measures to solve the problem of heat damage at the working face during deep mining mainly relies on practical experience.

The new method of “the ground cooling-deep underground long-distance borehole cooling-concentrated cooling in mining areas” can effectively solve the problem of cooling and heat dissipation in underground environments. The method can effectively shorten the cooling distance, improve the cooling efficiency, avoid installing the refrigeration unit downhole, and keep maintenance of the cooling system easy. However, when the chilled water from the ground is transported over long distances through deep strata to the underground mining area, the pipeline is subjected to extrusion and shear stresses caused by ground stress and the water flow, resulting in potential risks such as delamination, fracture, and leakage. In particular, the long-distance composite structure of the heat preservation and cold transfer pipe in the underground cooling of high-temperature mines should be considered in addition to the control of cold loss. What is more, other aspects should be considered, such as the mechanical properties of the solid pipe plugging filling material between the borehole and the casing and the insulation material between the casing and the cold-water transfer pipe, such as compressive and tensile resistance, the extrusion stress and shear stress caused by gravity and water strike of the casing, cold pipe, solid pipe plugging material, insulation material, and cold-water transmission. The

abovementioned items ensures the stability and reliability of the casing and long-distance cold transmission pipe in the borehole through deep strata.

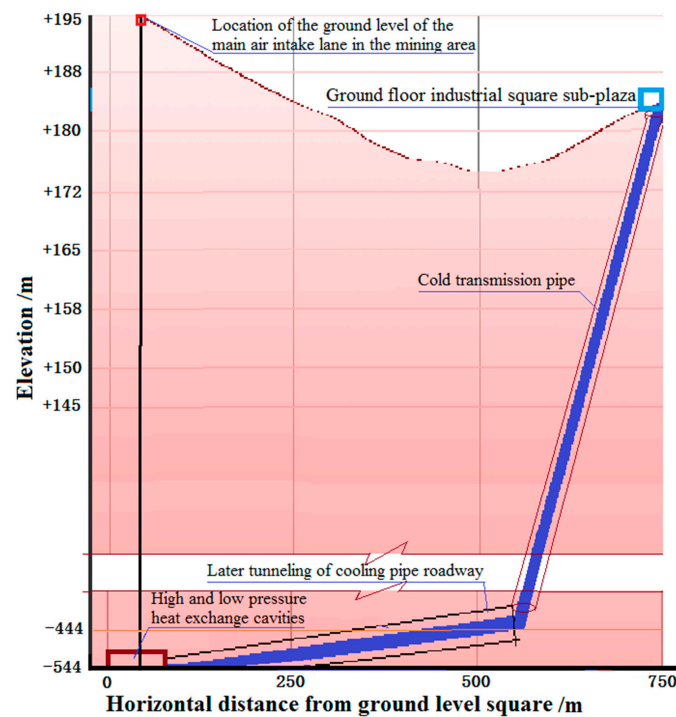
The insulation materials must also adapt to the special environment of high temperature and high humidity in high-temperature heat-damaged mines. Their protective layers must have enough strength to protect the insulation material from damage [20]. Currently, the most commonly used insulation materials include polystyrene and rigid polyurethane foamed. Yue et al. [21,22] improved the artificial system of chilled water cooling and proposed an integrated system concept of shallow geothermal heat storage, mine cooling, and a variable condition heat pump for the current situation of the high heat discharge and low utilization rate of the independent cooling system in mines, and they carried out relevant researches in the aspects of long distance transportation of chilled water and critical technology of centralized cooling with significant enthalpy difference. The results have been practically applied in engineering.

Zhu, H. et al. [23] studied the flow erosion and deformation of oil pipeline under the coupling effect of fluid and solid and analyzed the influencing factors of corrosion and deformation of the tee pipeline. The numerical results show that higher inlet mass flow or 90-degree confluence angle leads to more serious water flow erosion and larger deformation. Zhang, J. et al. [24] studied the mechanical behavior and plastic deformation of buried pipelines under soil overloading. The results show that the no-pressure pipeline is more prone to failure, and the von Mises stress and plastic strain of buried pipeline increase as the ground loading and loading area increase. Mou, B. et al. [25] studied the Seismic behavior of the corner joints of a frame under biaxial cyclic loading. The results indicate that the loading types affect the bearing capacities of the specimens. Wang, K. et al. [26] studied the mechanical properties of the long-distance energy transmission pipeline (LETP) under the interaction of temperature load and pressure load. The results show that the coupling of the temperature loading and the pressure loading is significantly affected by the end-side constraints of the pipelines. Qin, G. et al. [27] studied the pipeline condition assessment and finite-element modeling of mechano-electrochemical interaction between corrosion defects with varied orientations on pipelines. The results show that the strongest mechano-electrochemical interaction occurred between defects when the longitudinal or circumferential spacing is 0, causing high-level local stress concentration and the anodic current density (i.e., corrosion rate) at the corrosion defects. As the defects gradually overlapped or separated from each other on the pipe surface, the magnitude of the M E interaction decreased. The interaction between defects even disappeared when the longitudinal or circumferential spacing between defects reached 96 mm or 72 mm, respectively, and the defects can be assessed separately. From the above literature, it is found that the safety of the pipeline operation is determined by a variety of loadings. Moreover, the various physical fields generated by the different loadings are coupled with each other and jointly affect the stress and deformation of the pipeline, which ultimately determines the mechanical properties of the pipeline network.

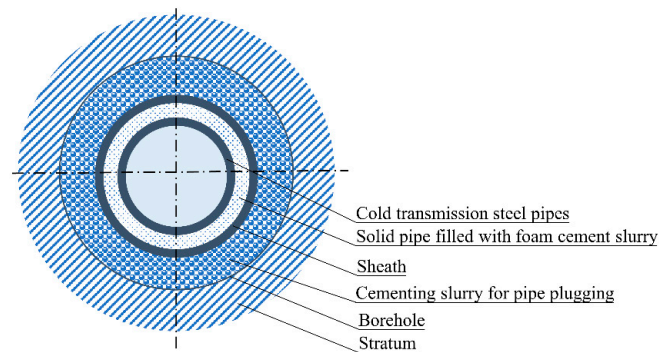
Based on the proposed selection of ordinary cement mortar (OCM) and insulation-foamed cement mortar (FCM) suitable for grouting construction between the cold transmission borehole, casing, and long-distance cold transmission pipeline in Wutongzhuang mine, Handan, trial grouting samplings were carried out to test the tensile and compressive properties of the cement slurry and insulation-foamed cement slurry specimens at normal temperature. By conducting uniaxial compression tests and Brazilian splitting mechanical tests and building FLAC3D finite-difference models, numerical simulations were adopted to investigate the overall stability and reliability of the long-distance composite insulation and cold transmission pipeline through deep strata. The results validated the feasibility of the new insulated cold transmission pipe with a composite structure, providing a theoretical basis for the design, installation, and operational safety of cold transmission pipelines through deep strata.

2. Engineering Background

The deep shaft under study is located in the Wutongzhuang mine in Handan, China. The depth of the inlet tunnel of the mining area is about 739 m. To reduce the loss of cold transmission, the distance of cold transmission should be the shortest, which can be achieved by setting a refrigeration station on the ground in the vertical direction of the underground heat exchange station. However, the ground in this location is the protected farmland, which is unsuitable for setting the refrigeration station, while 450 m to the northwest is an industrial sub-plaza of the mine, where a ground refrigeration station can be set up, and the correspondence relation in the vertical direction is shown in Figure 1a. The chilled water supply pipe and its installation borehole between the surface cooling station and the underground high and low-pressure heat exchange station are constructed with an oblique borehole passing through the strata. The vertical depth and the length of the chilled water supply pipe through the strata are approximately 630 m and 700 m.

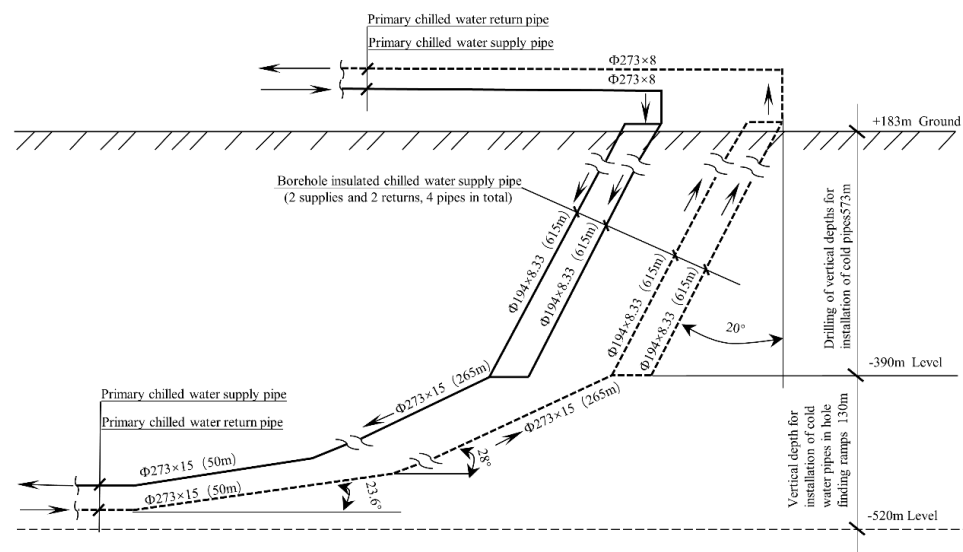


(a)



(b)

Figure 1. Cont.



(c)

Figure 1. Location cross-reference drawing, section, and layout of cold transmission pipes: (a) Comparison of the location of the industrial sub-plaza on the surface and the air intake lane in the underground mining area; (b) Cross-sectional view of insulated cold transmission pipe; (c) Insulated cold transmission pipe layout.

Except when affected by the heat transfer from the stratum with a certain temperature distribution, the cold pipe must have a certain mechanical strength to withstand various stress impacts and damages. Therefore, the cold transmission pipe needs to be designed to meet both the adiabatic insulation needs of the heat transfer and cold loss in the cold transfer process and the compressive strength requirements of the stress damage. The preliminary design of the composite insulation pipe structure is shown in Figure 1b. The layer from the inside to the outside is cold steel pipe, solid pipe filling cement slurry layer, cold pipe protection casing, solid pipe plugging cement slurry layer, and drilling, respectively. The cold transmission pipe is divided into the water supply and return pipe. As the cooling load is greater, the diameter of the cold transmission pipe is larger, which will inevitably cause the casing and borehole diameter to be larger. The larger diameter of cold transmission pipe and borehole brings huge difficulty and risk to drilling slant holes through deep strata while increasing the construction cycle. Therefore, the cold transmission system is composed of four cold transmission pipes: two are water supply pipes and two are return pipes, as shown in Figure 1. The heat transfer of the cold pipe through the deep strata directly affects the size of the loss in the process of cold-water transmission, and if the temperature rise is too large, it directly affects the cooling effect downhole.

3. Filling Material Mechanical Properties Tests

Based on the material mechanics experiment, we studied the stress state (uniaxial compression and uniaxial tension) of the solid pipe and insulation material in the cold transmission pipe. Additionally, we analyzed the uniaxial compressive and tensile properties of the filling material, such as the OCM material and FCM materials, which provided the basis for analyzing and evaluating the safety and stability of the composite cold transmission pipes.

3.1. Specimens Preparation and Testing Equipment

To investigate the compressive and tensile properties of the OCM specimens and insulated FCM specimens of hardened cold transmission pipe, specimens for uniaxial compression tests and Brazilian splitting tests were prepared by taking cores from the cold transmission pipe and using them, as shown in Figure 2. In this study, specimens were

processed into plates with height \times width \times thickness = 50 mm \times 30 mm \times 20 mm to make the full-field strain measurements more conducive.

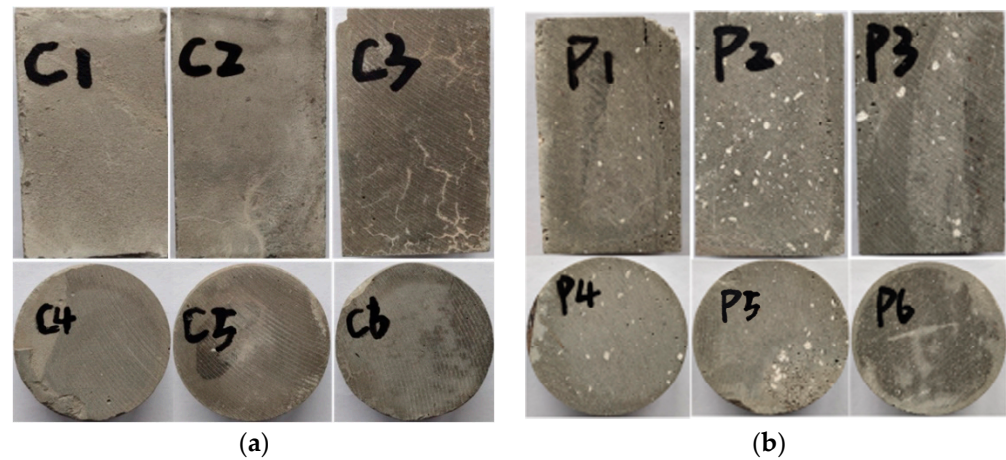


Figure 2. Ordinary cement and foamed cement specimens: (a) Ordinary cement mortar specimens; (b) Foamed cement mortar specimens.

The uniaxial compressive and tensile properties of ordinary and foamed cement mortar specimens were monitored by a DNS100 electronic universal testing machine from China University of Mining and Technology. A displacement-controlled loading mode with a 0.18 mm/min loading rate was used. To quantitatively study the strain field evolution process of the material under compression, a high-speed digital camera was used to take real-time pictures of the damage and fracture process of the specimens, and a digital image correlation system could be adopted to analyze the strain field distribution on the surface of the specimens. The layout of the specific experimental equipment is shown in Figure 3. Before loading, the specimens were first treated with laser speckle, as shown in Figure 3.

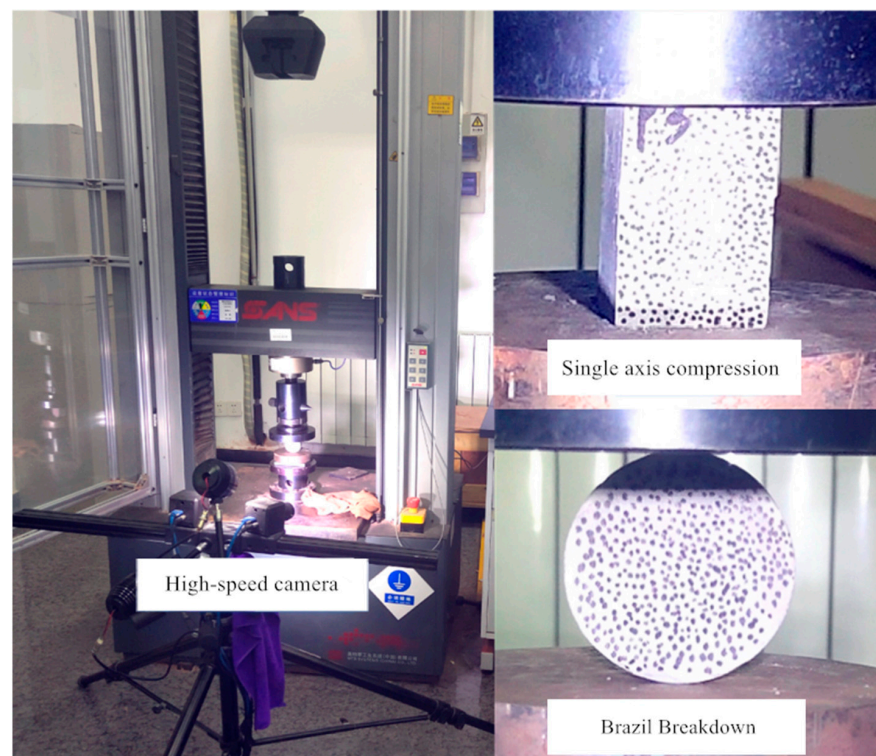
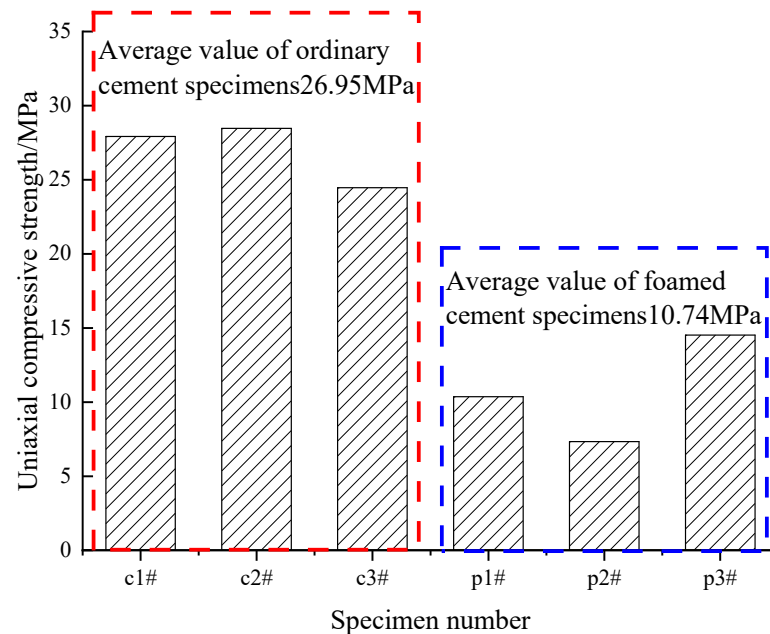


Figure 3. Equipment arrangement for uniaxial compression and Brazilian splitting tests.

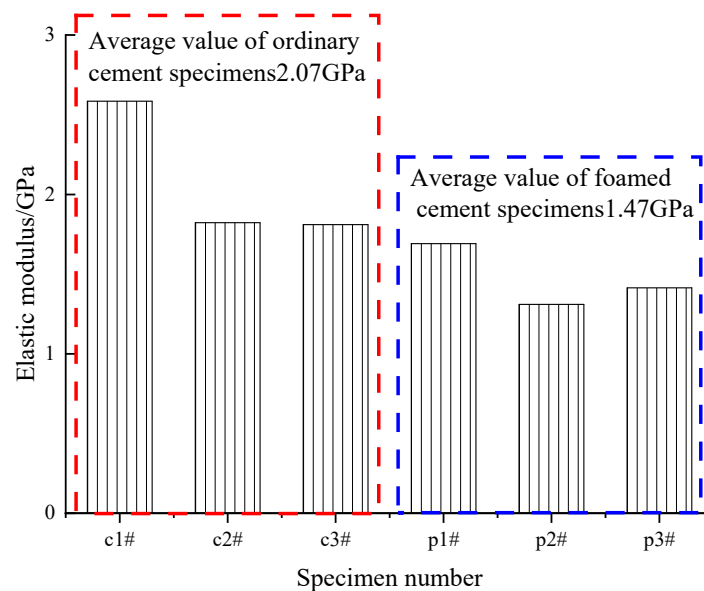
3.2. Results and Analysis

3.2.1. Uniaxial Compressive Properties of Filling Materials

The histograms of uniaxial compressive strength (UCS) and elastic modulus (E) of OC and FC specimens are shown in Figure 4.



(a)



(b)

Figure 4. Histogram of UCS and E of the filling material: (a) Uniaxial compressive strength; (b) Modulus of elasticity.

The evolution of the maximum strain under uniaxial compression of the filling material was obtained by analyzing the photographs taken by the high-speed camera during the uniaxial compression test with digital image correlation techniques, as shown in Figure 5. From left to right are 50% peak stress, 80% peak stress, 90% peak stress, 100% peak stress,

and the maximum principal strain distribution on the surface of the uniaxially compressed specimen after peak. Figure 5 shows that, for the OCM specimen, the maximum strain develops gradually from the lower right end of the specimen as the loading proceeds, and the maximum strain is only 2%. When the stress exceeds a certain value, the stress is concentrated in the upper right part of the specimen and develops continuously. Finally, a band area with the largest mean strain value appears in the central axis of the specimen and the specimen is damaged. The OCM material is brittle, and the damage is typical of brittle tensile damage. When stress is near the UCS, some of the surface scatter was detached from the specimens, affecting the calculation accuracy and the maximum principal strain of the actual rock sample could not reach 15%.

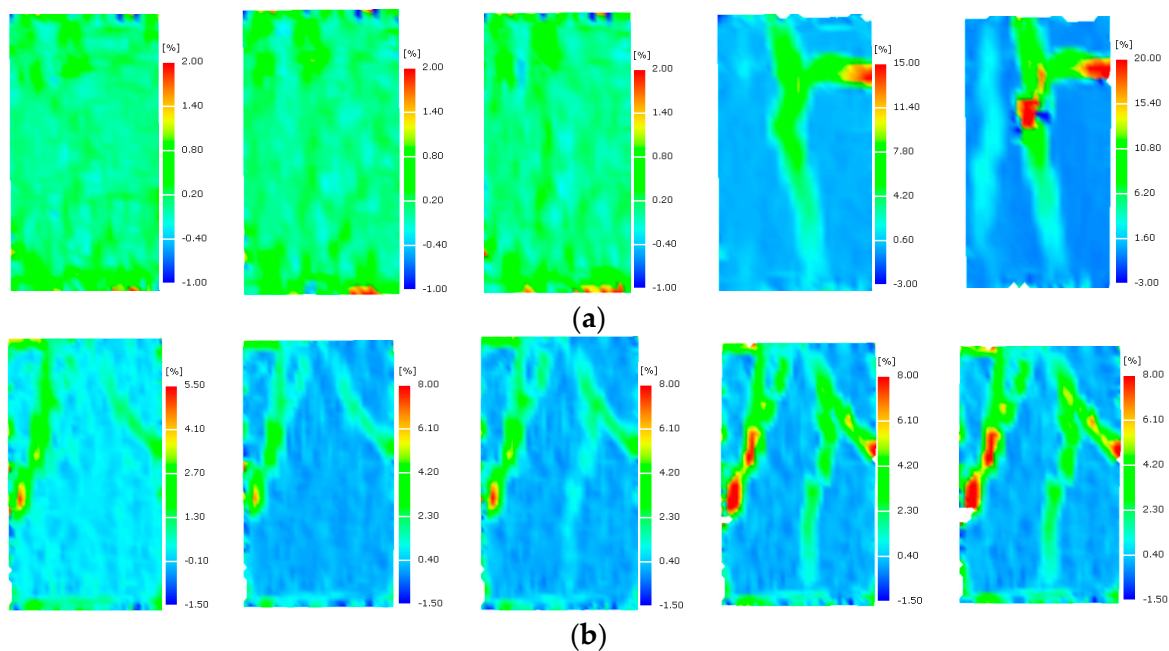


Figure 5. Evolution of the maximum principal strain under uniaxial compression of the filling material: (a) OCM specimens; (b) FCM specimens.

In the uniaxial compression process of the FCM specimen, two large strain zones appear at the left and right ends of the upper part of the specimen at the initial moment. With the stress increasing, these two zones develop. The third large strain zone appears when the stress exceeds a specific value. Eventually, all three large strain zones are destroyed at the time of damage: foamed cement mortar displays plastic characteristics compared to the OCM specimen and its damage is compression-shear damage. Through the study of the strain field of foamed concrete, it is found that foamed concrete has strong plastic failure characteristics, which is quite different from that of ordinary concrete. This research result is consistent with the research results of Lei-lei Guan et al. [28] on foamed concrete, and they all believe that foamed concrete has good plastic deformation ability.

3.2.2. Tensile Properties of the Filling Material

The column chart of the tensile strength of the filling materials is shown in Figure 6. It can be seen that the uniaxial tensile strengths of the OCM specimens are all higher than that of the foamed cement mortar, and the uniaxial tensile strengths of the OCM specimens are all higher than 2.09 MPa, with a more uniform distribution; the uniaxial tensile strengths of the foamed cement mortar are more discrete in distribution, and the uniaxial compressive strength of specimen P5# is twice that of P6#.

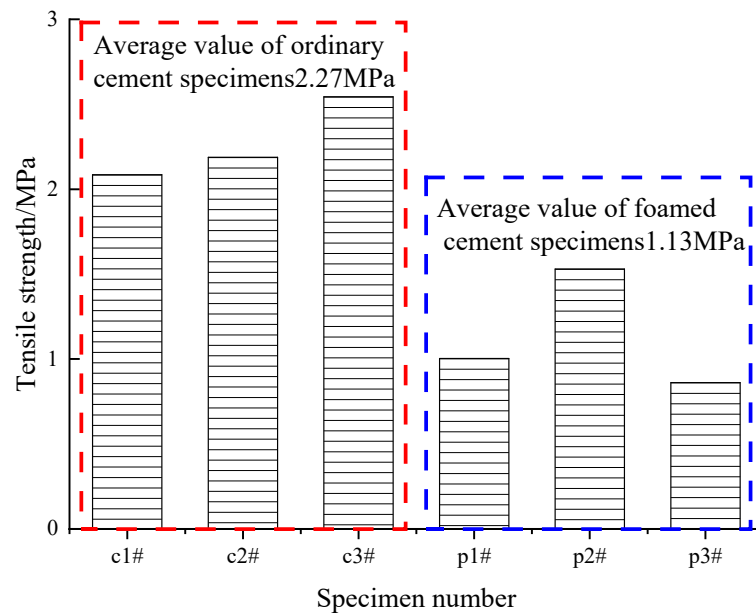


Figure 6. Histogram of tensile and compressive strength of the filling material.

Analyzing the photographs captured by a high-speed camera during the Brazilian splitting tests with digital image correlation techniques, the evolution of the maximum strain of the filling material was obtained.

As shown in Figure 7, from left to right, are 50% peak stress, 80% peak stress, 90% peak stress, 100% peak stress, and the maximum principal strain distribution on the surface of the uniaxially compressed specimen after peak. From Figure 7, it can be seen that under Brazilian splitting tests, the OCM specimens do not have an obvious larger strain zone in the vertical diameter direction, and only at the critical moment of damage a maximum principal strain line along the vertical diameter direction appears; under Brazilian splitting tests, the foamed cement mortar does not have an obvious characteristic of a maximum strain zone at lower stress levels, and after the stress exceeds a certain value, a larger principal strain zone appears along the vertical diameter direction and a fracture occurs at the center of the cylinder.

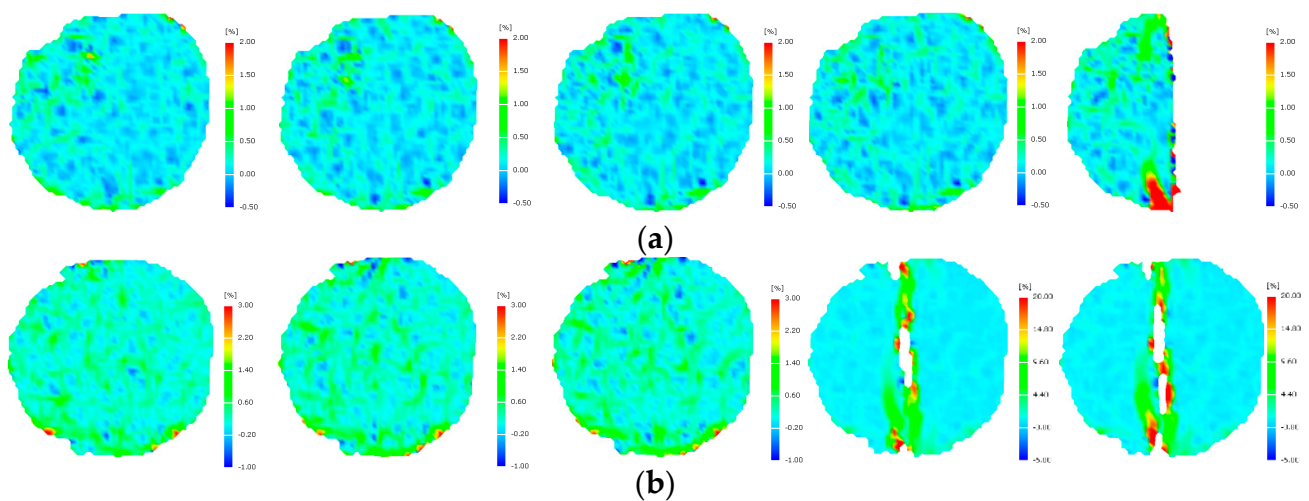


Figure 7. Evolution of the maximum principal strain in specimens under Brazilian splitting tests: (a) OCM specimens; (b) FCM specimens.

A comparison of the evolution of the maximum principal strains in ordinary cement paste and foamed cement paste under Brazilian split tests shows that the damage process

is different; the damage in ordinary cement paste is instantaneous, whereas in foamed cement paste the damage starts at the central point and the top and bottom, with fracture developing and penetrating gradually through the top and bottom and the central point.

4. Overall Stability of Insulated Cold Transfer pipes

4.1. Numerical Modeling

To study the mechanical state of the pipe wall under different burial depths and stratigraphic environments, FLAC3D numerical software was used to analyze the displacement, stress, and plastic zone conditions systematically. Combined with the actual geological conditions of the project, referring to the relevant literature and laboratory results, the inner diameter of the designed pipe envelope is 0.38 m, and the model side length is not less than 1.14 m according to the Saint-Venant’s principle. Therefore, a square of size 1.4 m × 1.4 m × 1.4 m was selected for the numerical simulation. The composite insulation and cold transmission pipeline through deep strata were arranged in the center of the model, which could radiate outward evenly. The inner wall of the pipe has a diameter of 97 mm and a thickness of 9 mm; the inner cement is foamed cement paste with a thickness of 30 mm; the outer cement is ordinary cement paste with a thickness of 45 mm; between the two layers of cement is the steel pipe with a thickness of 9 mm; the ordinary cement paste is in direct contact with the rock and soil mass of the surrounding rock.

The meshed numerical model is shown in Figure 8. Mesh encryptions were carried out for the internal part of ordinary cement paste, foamed cement paste, and steel pipe in order to obtain a precise analysis result. To improve the calculation efficiency, the external surrounding rock mesh size is larger, and the model has 4800 meshes and 9760 nodes. The numerical model parameters are shown in Table 1.

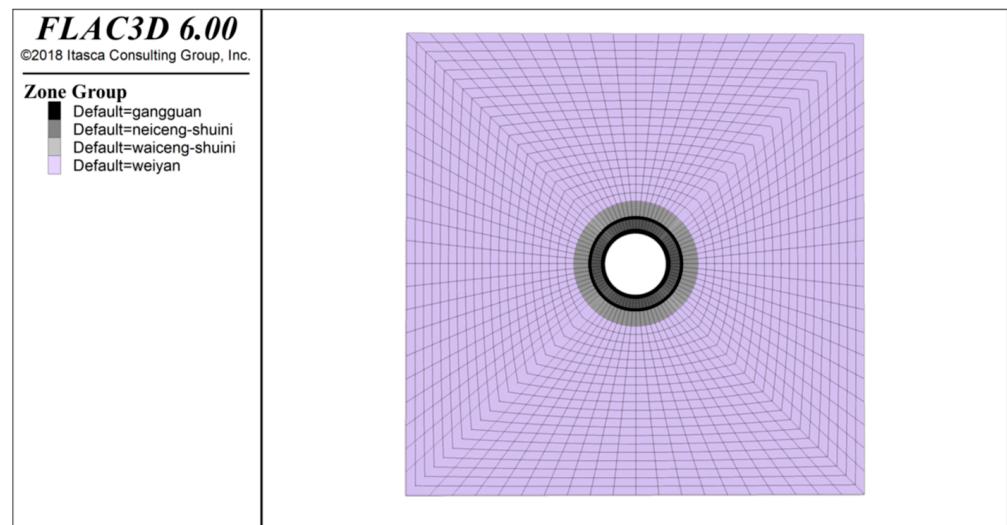


Figure 8. Schematic diagram of the FLAC3D model and survey line layout.

Table 1. Numerical model parameter.

	Bulk Density/g/cm ³	Compressive Strength/MPa	Tensile Strength/MPa	Elastic Modulus/GPa	Shear Modulus/GPa	Poisson's Ratio	Cohesion/MPa	Internal Friction Angle/°
Steel pipe	7.82	235	450	220	80	0.29	900	45
Mudstone	2.46	18.29	1.82	2.63	3.35	0.23	1.71	29.65
Foam concrete	0.98	1.13	0.10	1.47	0.61	0.2	1.8	38
Ordinary concrete	2.4	2.27	0.25	2.07	0.86	0.2	2.3	43.5

To quantitatively analyze the displacement and stress attenuation law of the composite insulated cold transmission pipe through the deep strata and the surrounding rock under deep ground stress, 24 measurement points were arranged in the vertical direction of the model from inside to outside, and their vertical displacement, axial stress, and tangential stress under different ground stress conditions were monitored. Both the two steel pipes

were placed evenly with 3 points at 3 mm intervals, the FCM with 5 points at 6 mm intervals, the OCM with 8 points at 6 mm intervals and the rock and soil mass with 5 points at 10 mm intervals.

The Mohr–Coulomb criterion was used in the simulations to determine the deformation and yielding of the surrounding rock and the borehole insulation pipe. A total of six ground stress scenarios, namely 3 MPa, 6 MPa, 9 MPa, 12 MPa, 15 MPa and 17.5 MPa, were used to simulate the ground stresses on the insulation pipe from +183 m to −520 m. Displacement boundary conditions were applied at the boundary of the calculation model and then a gradient loading method was set to load the stresses, and when the horizontal and vertical stresses were loaded to set ground stresses, the loading stresses were stopped and iterative equilibration began.

4.2. Stability of the Surrounding Rock on the Outside of the Cold Transmission Pipe

The vertical displacement of the surrounding rock above the insulated cold pipe at different distances from the inner wall of the steel pipe is shown in Figure 9. It can be seen that when the ground stress is 3 MPa, the vertical displacement of the surrounding rock within the range of 40 mm measurement points almost does not change, which is approximately equal to 0. Due to the homogeneity of the nature of the model surrounding rock, the vertical displacement of the surrounding rock decreases linearly with the increase in the distance from the inner wall of the steel pipe. With the increasing ground stress, the vertical displacement of the surrounding rock also gradually increases. When the ground stress is 17.5 MPa, the vertical deformation of the surrounding rock around the pipe reaches about 0.12 mm, and the difference of vertical displacement within 40 mm is about 0.02 mm.

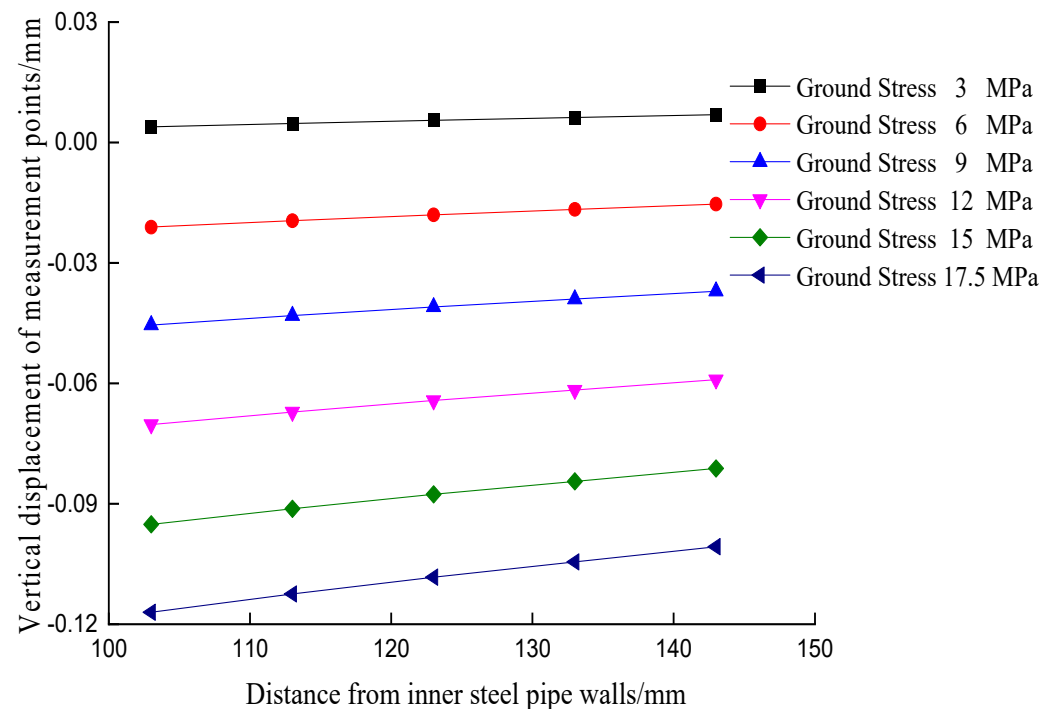


Figure 9. Variation of vertical displacement of the surrounding rock measurement points with distance from the inner steel pipe wall.

Figure 10 shows the vertical stress distribution contour and the axial and tangential stress curves at the measurement points of the surrounding rock with the distance from the inner wall of the steel pipe under different ground stress conditions for the composite insulated cold transmission pipe trough deep strata.

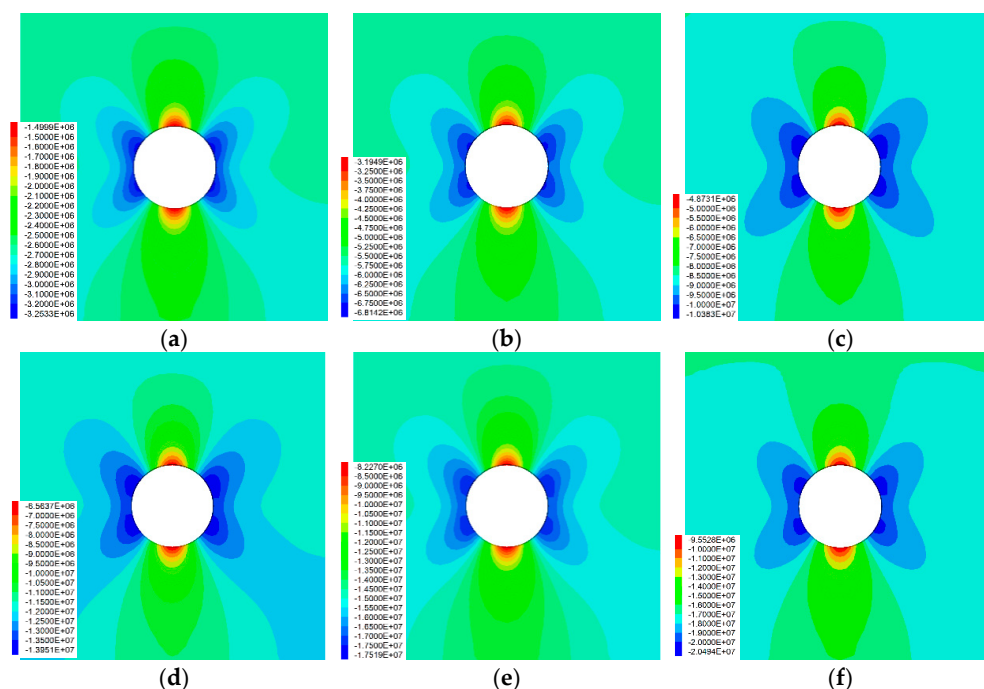


Figure 10. Distribution of vertical stresses in the external surrounding rock under different ground stress conditions: (a) 3MPa; (b) 6MPa; (c) 9MPa; (d) 12MPa; (e) 15MPa; (f) 17.5MPa.

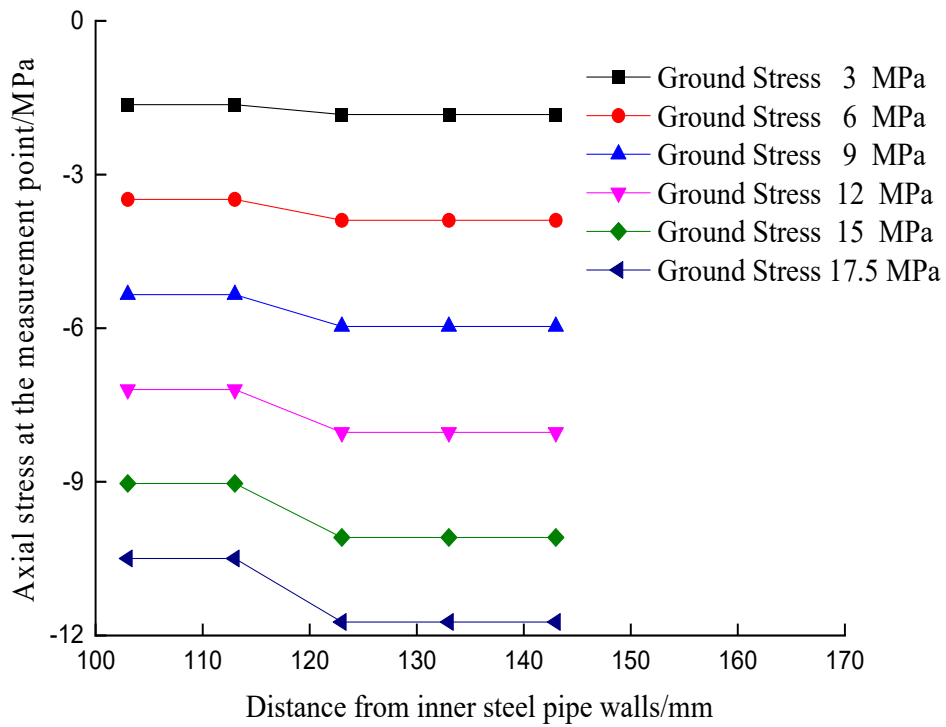
Under the conditions of ground stress, the axial stress distribution of the external rock surrounding the composite insulated cold transmission pipe through deep strata is butterfly-shaped, while the stress concentration mainly occurs on the left and right sides of the pipe. The axial stress on the left and right sides is generally greater than on the upper and lower sides. The stress concentration is most obvious at the four corner positions of the upper left, lower left, upper right, and lower right, and the axial stress on the upper and lower sides is relatively small. Table 2 presents the maximum vertical stress values of the external surrounding rock under different in situ stress conditions, where the negative sign indicates compressive stress. From Table 2, it can be observed that the maximum vertical stress of the external surrounding rock gradually increases with the increase in in situ stress. This finding is similar to that of Leng X. et al [29]. They found that with the rise of the shaft depth and stress coefficient under the different surrounding rock grades, the radial and tangential stress showed an increasing trend, but the growing trend was relatively gentle.

Table 2. Maximum vertical stress of external surrounding rock under different in situ stress conditions.

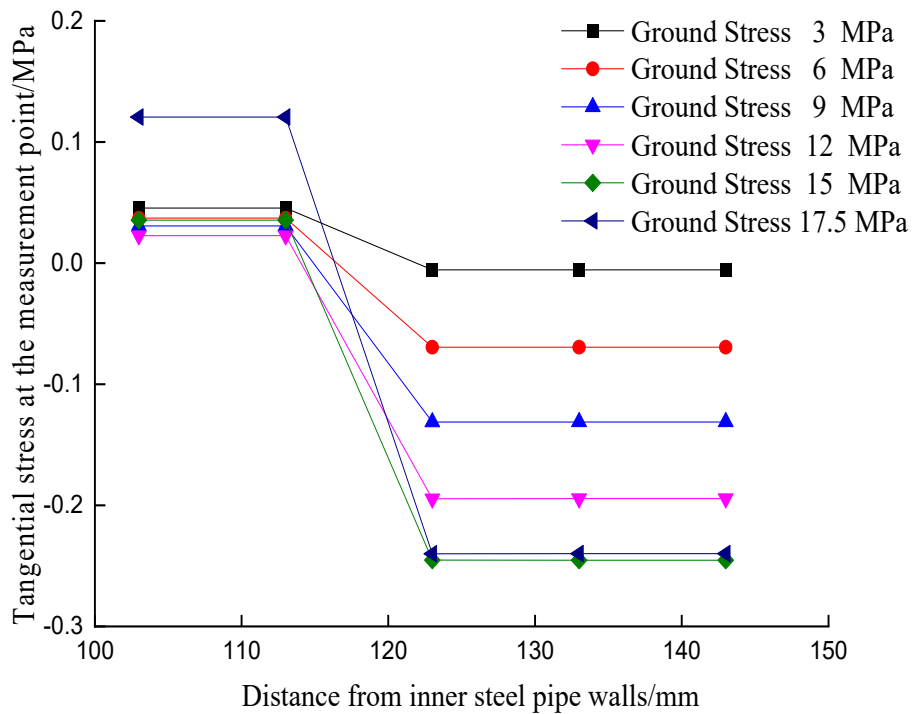
In-Situ Stress/MPa	Maximum Vertical Stress/MPa
3	−1.49
6	−3.19
9	−4.87
12	−6.58
15	−8.22
17.5	−9.55

Figure 11 shows the variation of the axial stress at the measurement point in the surrounding rock with the distance from the inner steel pipe wall. At ground stresses greater than 9 MPa, there is a slightly abrupt change in the distance from the inner steel pipe wall between 113 mm and 123 mm, and then gradual stabilization occurs. The same can be seen in the curve of tangential stresses in the surrounding rock with distance from the inner steel pipe wall, where there is an abrupt change in tangential stresses downwards as the distance from the measurement point increases from 113 mm to 123 mm. It can be

assumed that the effect of ground stress on the external rock is also zoned, with 113–123 mm being the critical zone.



(a)



(b)

Figure 11. Variation of axial and tangential stresses at the measurement points in the surrounding rock with distance from the inner steel pipe wall: (a) Axial stress, (b) Tangential stress.

4.3. Overall Structural Stability of Long-Distance Insulated Cold Transmission Pipes

The overall stability of the structure of the insulated cold transmission pipe directly affects the safety and stability of the operation of the insulated cold pipe in passing through the deep strata for the ground cooling system. Therefore, analyzing the displacement, stress, and plasticity zones is particularly important. The vertical displacement contour of the pipe under different ground stress conditions shows that the displacement of the pipe mainly occurs at the upper and lower walls of the pipe and decreases outwards layer by layer. At the same time, there is almost no vertical displacement on both sides of the pipe.

Figure 12 shows that when the ground stress is 3 MPa and 6 MPa, there is almost no vertical displacement between the inner steel pipe and the cement, and the deformation of the whole pipe is minimal. When the ground stress exceeds 6 MPa, the vertical displacement of the inner steel pipe is significantly higher than that of the outer steel pipe and the layer of cement. Under high-ground stress, the deformation of the unit thickness of the FCM is much higher than that of the OCM. Meanwhile, there is almost no deformation of the steel pipe, and the deformation of the insulated pipe mainly comes from the deformation of the cement material. As the ground stress increases, the vertical displacement of the steel pipe, OCM, and FCM all increase linearly. The change in vertical displacement of the inner steel pipe is mostly influenced by the ground stress, and the OCM is least influenced by the ground stress.

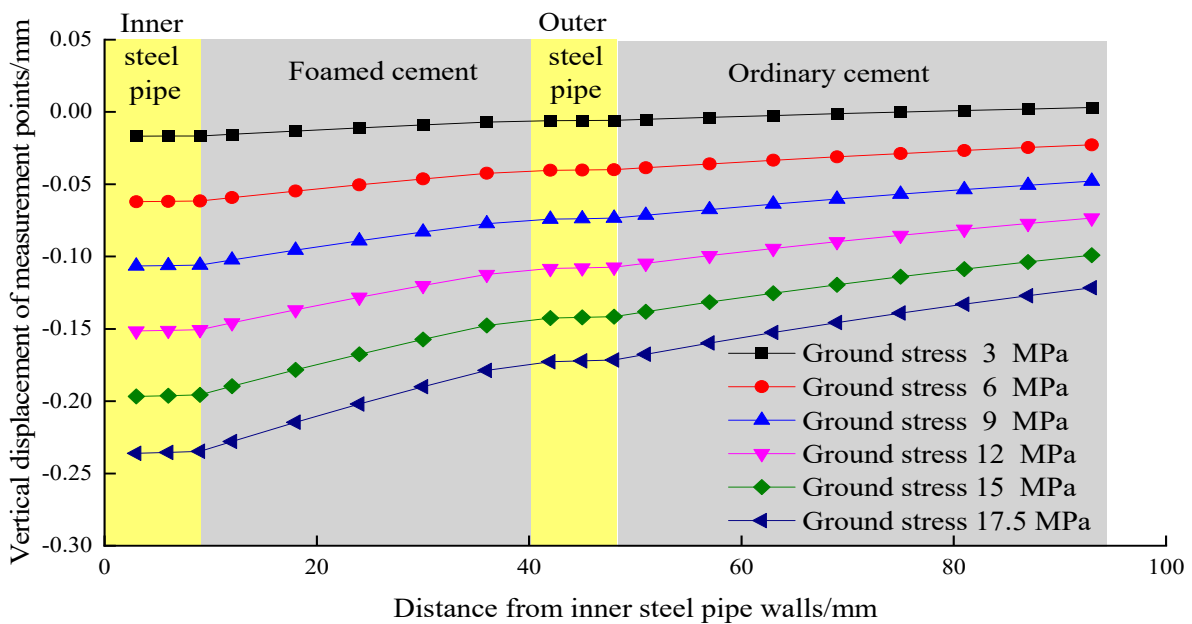


Figure 12. Variation of vertical displacement of insulated cold transmission pipe at measurement points with distance from the inner pipe wall.

The axial stress distribution of the insulated cold transmission pipe under different ground stress conditions is shown in Figure 13, from which it can be seen that the largest zone of the insulated cold transmission pipe subjected to axial stress is the left and right sides, and the two layers of steel pipe bear more stress concentration, relieving the stress concentration in the OCM and FCM. Under high-ground stress conditions, the stress distribution of the insulated cold transmission pipe is as follows: the left and right inner walls of the pipe are the largest, the inner walls of the four corners are the second largest, and the upper and lower inner walls are the smallest.

Figure 14 shows the different parts of the insulated cold transmission pipes with the distance from the inner steel pipe wall and the change in ground stress. As can be seen from the figure, the distance from the inner steel pipe wall and ground stress has the smallest impact on the axial direction of the inner steel pipe, and with the increase in ground stress, the axial stress of the inner steel pipe almost has no change, which is about

0 MPa, indicating that the inner steel pipe is almost not subject to axial stress. At this time, the inner part of insulated pipe can operate normally. When the distance from the inner wall of the steel pipe exceeds 9 mm, the axial stress of the insulation pipe increases linearly with the distance, and the OCM and FCM have the essential roles in the attenuation and dissipation of the axial stress. As the ground stress increases, the OCM is most affected by the axial stress and the inner steel pipe is least affected by the axial stress.

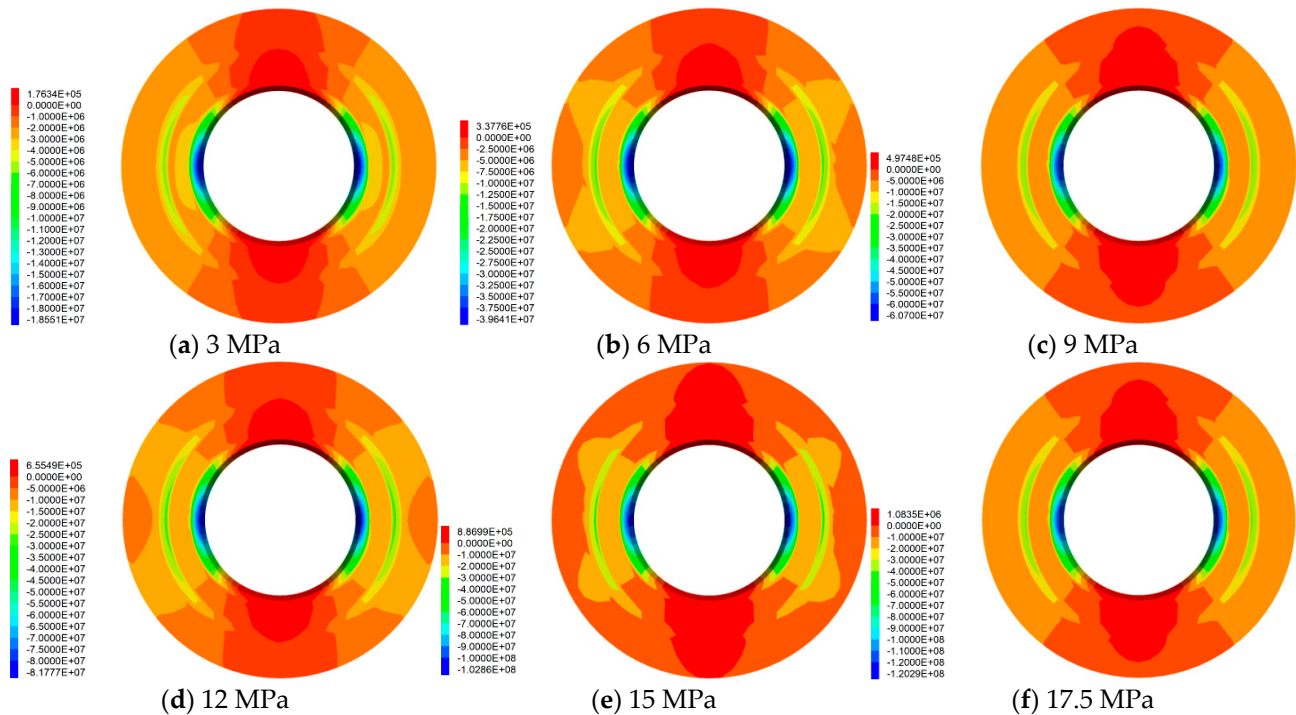


Figure 13. Axial stress distribution of insulated cold transmission pipes under different ground stress conditions.

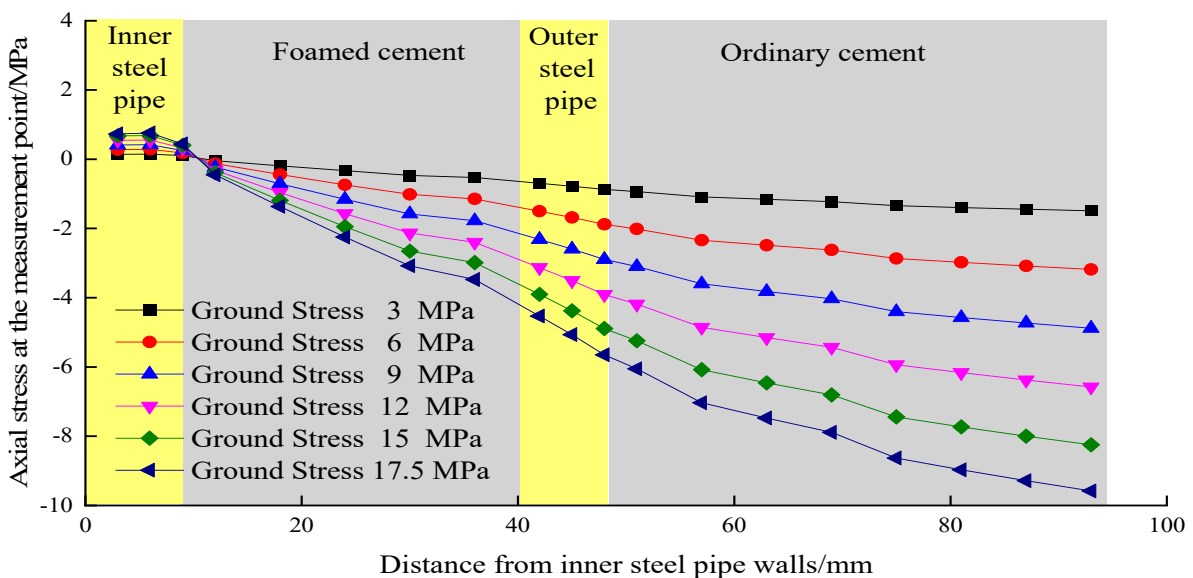


Figure 14. Variation of the axial stress at the measurement point of an insulated cold pipe with distance from the inner pipe wall.

Figure 15 shows the distribution of the plastic zone in different parts of the insulated cold transmission pipe under different ground stress conditions. The figure shows no

yielding in the plastic zones of the insulated cold transmission pipe when the ground stress ranges from 3 MPa to 12 MPa. When the ground stress reaches 15 MPa, yielding starts to occur in the insulated cold transmission pipe, with the four corners of the pipe showing tension-p, which indicates tensile yielding has occurred at these locations. As the ground stress increases to 17.5 MPa (a value equal to the conventional ground stress magnitude at 700 m depth), the yielding failure of the pipe still occurs mainly at the corners, showing significant tensile yielding and a small amount of shear yielding. However, although there is a partial plastic zone in the insulated pipe at 15 MPa and 17.5 MPa, the plastic zone mainly occurs at the OCM and FCM filling materials, and the plastic zone is small, which does not affect the regular working operation of the insulated pipe. The insulated cold transmission pipe of the composite structure through the deep strata from the inside to the outside is composed of cold pipe, insulation-foamed cement paste layer, metal protection casing, solid pipe plugging cement layer outside casing, and borehole rock layer. The insulated cold transmission pipe, insulation cement layer, and casing are fixed through the solid pipe plugging cement layer outside the casing, forming the mechanical properties of the composite structure. Accordingly, the calculation simulation analysis of the overall strength of the cold pipe is reliable, which can ensure the safe and stable operation.

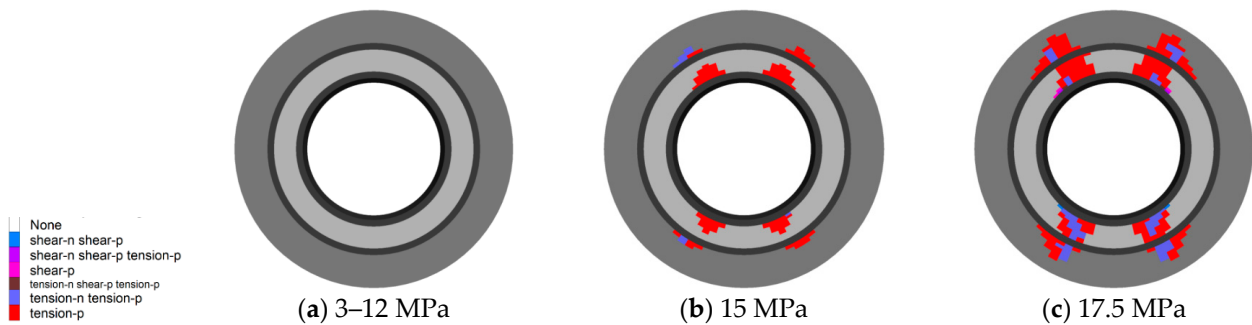


Figure 15. Distribution of plastic zones in different parts of insulated cold pipe under different ground stress conditions.

The plastic damage distribution characteristics of the outer solid pipe material and the inner insulation layer under different ground stress conditions are shown in Figure 16. When the ground stress is less than or equal to 12 MPa, the material does not show plastic damage, and when it is beyond 12 MPa, the plasticity rate generally shows an increasing linear trend. Therefore, Equations (1) and (2) can be used to express the plasticity damage rate of the outer material and the inner insulation layer, respectively.

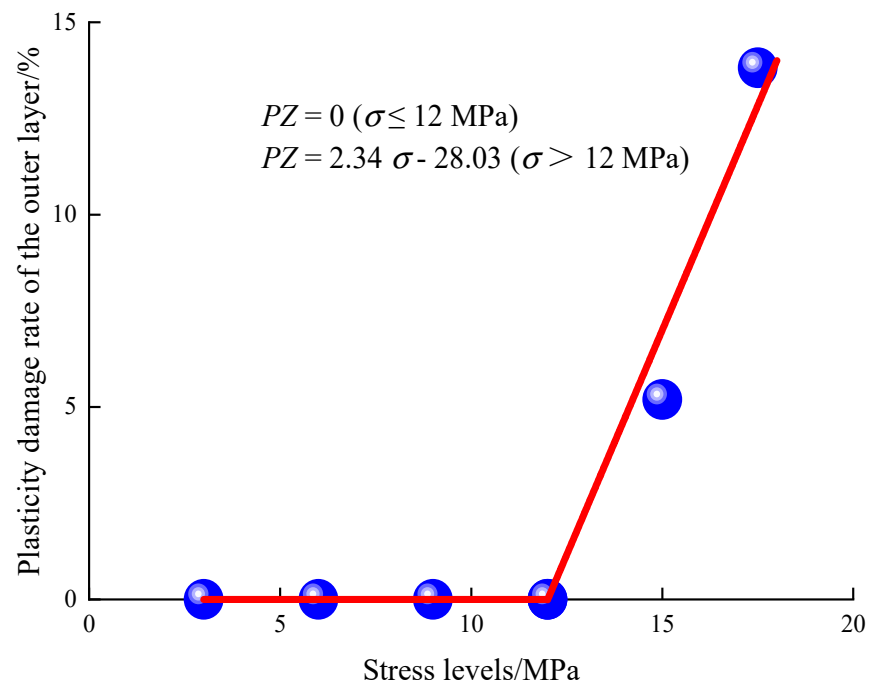
$$PZ = \begin{cases} 0 & (\sigma \leq 12 \text{ MPa}) \\ 2.34\sigma - 28.03 & (\sigma > 12 \text{ MPa}) \end{cases} \tag{1}$$

$$PZ = \begin{cases} 0 & (\sigma \leq 12 \text{ MPa}) \\ 6.52\sigma - 78.28 & (\sigma > 12 \text{ MPa}) \end{cases} \tag{2}$$

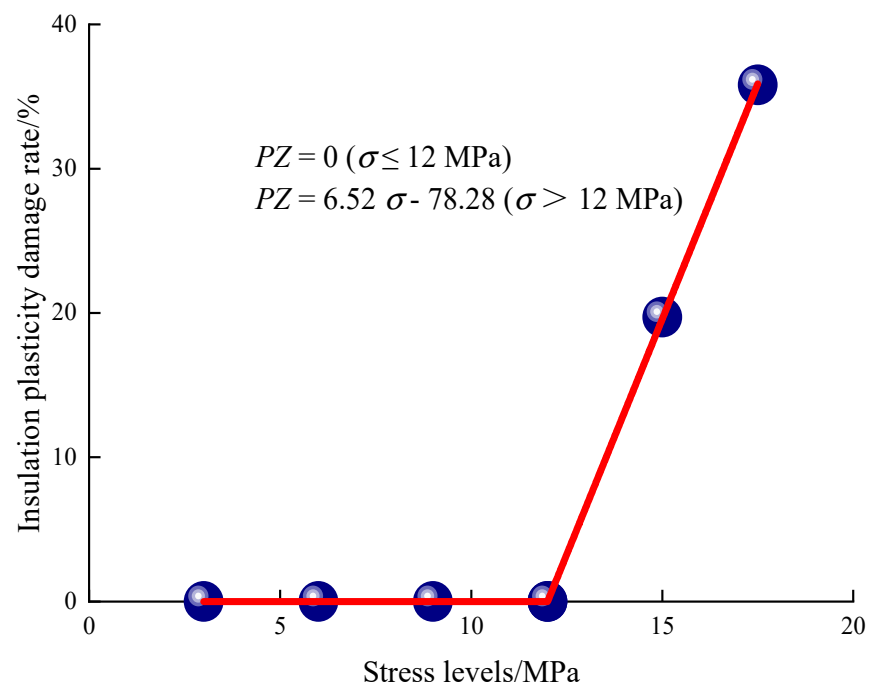
where PZ is the plasticity damage rate, and σ is the ground stress level. The destruction of the material will also be affected by the size of the insulation pipe, geometry, material properties, and other factors. Equations (1) and (2) can be simplified as

$$PZ = \begin{cases} 0 & (\sigma \leq 12 \text{ MPa}) \\ a \cdot \sigma_0 - 78.28b & (\sigma > 12 \text{ MPa}) \end{cases} \tag{3}$$

where σ_0 is the critical stress level, and a and b are the physical parameters.



(a)



(b)

Figure 16. Plastic zone proportion of insulated cold pipe materials, (a) Outer layer, (b) Internal insulation.

5. Conclusions

Uniaxial compression tests and splitting tests were carried out to address the problems of delamination and water leakage caused by the fracture of the cold transmission pipeline during the long-distance drilling of deep wells. The distribution law of the maximum

principal strain field on the surface of the filling mortar was obtained based on digital image analysis. A FLAC3D finite-difference model was established and calculated to study the deformation and damage characteristics of the long-distance composite insulated cold transmission pipeline under different stress conditions. The main conclusions obtained are as follows.

(1) The uniaxial compressive strength, modulus of elasticity, and Brazilian splitting strength of ordinary cement mortar (OCM) specimens were higher than those of foamed cement mortar (FCM) specimens. Under uniaxial compression, the OCM specimens showed axial tensile damage, while the FCM specimens showed mixed compression-shear damage. Under Brazilian splitting, both the OCM and FCM specimens showed typical splitting damage.

(2) The axial stress distribution of the surrounding rock outside the pipe is butterfly-shaped, and the stress concentration mainly occurs on the left and right sides of the pipe. With the increase in the ground stress, the OCM is most affected by the axial stress, and the inner steel pipe is least affected by the axial stress. When the ground stress is large, there is a sudden change in the tangential stress between 113 mm and 123 mm from the inner steel pipe wall.

(3) The ground stress has a significant effect on the overall structural stability of the long-distance insulated cold transmission pipe. When the ground stress is small (12 MPa), the material does not show plastic damage, and when the ground stress exceeds 12 MPa, the plasticity rate shows an overall linear increasing trend.

(4) The equations were derived for the plasticity damage rate and stress of the inner and outer sides of the cold transmission pipe filled with mortar. The parameters of the insulated pipe were constructed to provide a theoretical basis for enhancing the deformation and damage characteristics of the cold transmission pipe of the composite structure.

Author Contributions: W.W.: Investigation, Validation, Methodology, Software, Formal analysis, Data curation, Writing—original draft. F.Y.: Validation, Writing—review & editing. J.W.: Supervision, Conceptualization, Investigation, Writing—review & editing. T.G.: Validation, Conceptualization, Writing—review & editing. Y.Q.: Conceptualization, Investigation. All authors have read and agreed to the published version of the manuscript.

Funding: This research received no external funding.

Institutional Review Board Statement: Not applicable.

Informed Consent Statement: This study did not involve human studies.

Data Availability Statement: Data will be made available on request.

Conflicts of Interest: The authors declare that they have no known competing financial interest or personal relationship that could have appeared to influence the work reported in this paper.

References

1. Sasmito, A.P.; Kurnia, J.C.; Birgersson, E.; Mujumdar, A.S. Computational evaluation of thermal management strategies in an underground mine. *Appl. Therm. Eng.* **2015**, *90*, 1144–1150. [[CrossRef](#)]
2. Wang, Y.-J.; Zhou, G.-Q.; Wu, L. Unsteady heat-moisture transfer of wet airway in deep mining. *J. Cent. South. Univ.* **2013**, *20*, 1971–1977. [[CrossRef](#)]
3. del Castillo, D. Air cycle refrigeration system for cooling deep mines. *Int. J. Refrig.* **1988**, *11*, 87–91. [[CrossRef](#)]
4. Chen, W.; Liang, S.; Liu, J. Proposed split-type vapor compression refrigerator for heat hazard control in deep mines. *Appl. Therm. Eng.* **2016**, *105*, 425–435. [[CrossRef](#)]
5. Guo, P.; He, M.; Zheng, L.; Zhang, N. A geothermal recycling system for cooling and heating in deep mines. *Appl. Therm. Eng.* **2017**, *116*, 833–839. [[CrossRef](#)]
6. van der Walt, J.; de Kock, E.M. Developments in the engineering of refrigeration installations for cooling mines. *Int. J. Refrig.* **1984**, *7*, 27–40. [[CrossRef](#)]
7. Qi, P.; Manchao He Li, M.; Chen, C. Working principle and application of HEMS with lack of a cold source. *Chin. J. Min. Sci. Technol.* **2011**, *21*, 433–438. [[CrossRef](#)]
8. du Plessis, G.E.; Liebenberg, L.; Mathews, E.H. Case study: The effects of a variable flow energy saving strategy on a deep-mine cooling system. *Appl. Energ.* **2013**, *102*, 700–709.

9. Du Plessis, G.E.; Liebenberg, L.; Mathews, E.H.; Du Plessis, J.N. A versatile energy management system for large integrated cooling systems. *Energ. Convers. Manag.* **2013**, *66*, 312–325. [[CrossRef](#)]
10. Bornman, W.; Dirker, J.; Arndt, D.C.; Meyer, J.P. Integrated energy simulation of a deep level mine cooling system through a combination of forward and first-principle models applied to system-side parameters. *Appl. Therm. Eng.* **2017**, *123*, 1166–1180. [[CrossRef](#)]
11. Bahadori, A.; Vuthaluru, H.B. A simple method for the estimation of thermal insulation thickness. *Appl. Energ.* **2010**, *87*, 613–619. [[CrossRef](#)]
12. Daouas, N.; Hassen, Z.; Aissia, H.B. Analytical periodic solution for the study of thermal performance and optimum insulation thickness of building walls in Tunisia. *Appl. Therm. Eng.* **2010**, *30*, 319–326. [[CrossRef](#)]
13. Ozel, M. Thermal performance and optimum insulation thickness of building walls with different structure materials. *Appl. Therm. Eng.* **2011**, *31*, 3854–3863. [[CrossRef](#)]
14. Brecani, R.; Dervishi, S. Thermal and energy performance evaluation of underground bunkers: An adaptive reuse approach. *Sustain. Cities Soc.* **2019**, *46*, 101444. [[CrossRef](#)]
15. Wagner, H. The management of heat flow in deep mines. *Geomech. Tunn.* **2013**, *4*, 157–163. [[CrossRef](#)]
16. Wang, Y.; Wang, C.; Gao, S.; Zheng, X.; Darkwa, J. The impact of thermal insulation on cooling energy consumption and optimal insulation thickness for underground tunnel. *Sustain. Energy Technol. Assess.* **2021**, *47*, 101495. [[CrossRef](#)]
17. Crawford, J.A.; Joubert, H.P.R.; Mathews, M.J.; Kleingeld, M. Optimised dynamic control philosophy for improved performance of mine cooling systems. *Appl. Therm. Eng.* **2019**, *150*, 50–60. [[CrossRef](#)]
18. He, M.C. Application of HEMS cooling technology in deep mine heat hazard control. *Min. Sci. Technol.* **2009**, *19*, 269–275. [[CrossRef](#)]
19. Feng, X.P.; Jia, Z.; Liang, H.; Wang, Z.; Wang, B.; Jiang, X.; Cao, H. A Full Air Cooling and Heating System Based on Mine Water Source. *Appl. Therm. Eng.* **2018**, *145*, 610–617. [[CrossRef](#)]
20. Zhang, L.; Du, B.-C.; Gui, K.-W. Research on pipeline cooling technology for mine cooling system. *Chin. J. Xiangtan Min. Inst.* **1992**, *S1*, 23–30.
21. Yue, F.-T.; Liu, C.-Y.; Wei, J.-S.; Gao, T.; Wu, X.-H. Energy Consumption Analysis and Optimization of Mine Cooling System During Mine Construction. *Chin. J. Coal Sci. Technol.* **2014**, *42*, 57–60.
22. Wei, J.-S.; Yue, F.-T. Optimized Design and Application of Refrigeration System with Multi-Function Varied Performance Heat Pump Unit. *Chin. J. Coal Eng.* **2014**, *46*, 36–40.
23. Zhu, H.; Zhang, W.; Feng, G.; Qi, X. Fluid–structure interaction computational analysis of flow field, shear stress distribution and deformation of three-limb pipe. *Eng. Fail. Anal.* **2014**, *42*, 252–262. [[CrossRef](#)]
24. Zhang, J.; Liang, Z.; Zhao, G. Mechanical behaviour analysis of a buried steel pipeline under ground overload. *Eng. Fail. Anal.* **2016**, *63*, 131–145. [[CrossRef](#)]
25. Mou, B.; Li, X.; Qiao, Q.; He, B.; Wu, M. Seismic behaviour of the corner joints of a frame under biaxial cyclic loading. *Eng. Struct.* **2019**, *196*, 109316. [[CrossRef](#)]
26. Wang, K.; Xie, K.; Zhang, H.; Qiang, Y.; Du, Y.; Xiong, Y.; Zou, Z.; Zhang, M.; Zhong, L.; Akkurt, N.; et al. Numerical evaluation of the coupled/uncoupled effectiveness of a fluid-solid-thermal multi-field model for a long-distance energy transmission pipeline. *Energy* **2022**, *251*, 123964. [[CrossRef](#)]
27. Qin, G.; Huang, Y.; Wang, Y.; Frank Cheng, Y. Pipeline condition assessment and finite element modeling of mechano-electrochemical interaction between corrosion defects with varied orientations on pipelines. *Tunn. Undergr. Space Technol.* **2023**, *136*, 105101. [[CrossRef](#)]
28. Guan, L.; Chen, Y.; Ye, W.; Wu, D.; Deng, Y. Foamed concrete utilizing excavated soil and fly ash for urban underground space backfilling: Physical properties, mechanical properties, and microstructure. *Tunn. Undergr. Space Technol.* **2023**, *134*, 104995. [[CrossRef](#)]
29. Leng, X.-Q.; Yan, J.-X.; Han, Y.-X. Research on Influence of Ground Stress on the Stability of Deep and Large Shafts. *Chin. J. Undergr. Space Eng.* **2020**, *16*, 1451–1458+1483.

Disclaimer/Publisher's Note: The statements, opinions and data contained in all publications are solely those of the individual author(s) and contributor(s) and not of MDPI and/or the editor(s). MDPI and/or the editor(s) disclaim responsibility for any injury to people or property resulting from any ideas, methods, instructions or products referred to in the content.